

Corn straw-derived porous carbon as negative-electrode materials for lithium-ion batteries

Li-lai Liu¹, Min-xuan Ma^{1,*}, Yi-han Sun¹, Hui Wang¹, Xue-ying Yang¹, Ming-yang Li¹, Pan-di Wu²

¹ School of Environmental and Chemical Engineering, Heilongjiang University of Science and Technology, Harbin 150022, China.

² School of Foreign Studies, Harbin Engineering University, Harbin 150006, China

*E-mail: 346083403@qq.com

Received: 7 July 2022 / Accepted: 22 August 2022 / Published: 10 September 2022

The corn straw-based porous carbon prepared by KOH activation (K-TBC) has a hierarchical porous structure and a comparable specific surface area ($2357 \text{ m}^2 \text{ g}^{-1}$). These micro-mesoporous structures can facilitate the transport of electrolyte ions and exposure to more active sites. Electrochemical analysis shows that the reversible specific capacity of biomass carbon activated by KOH is 358 mAh g^{-1} , which is much higher than that of the negative electrode material without an activator. Due to the influence of the Solid Electrolyte Interphase (SEI) film, after 100 cycles at 0.1 A g^{-1} , the charge capacity of the lithium-ion battery prepared with K-TBC as the active material is merely 167 mA hg^{-1} but still better than that of the unactivated biomass carbon.

Keywords: corn straw, hierarchical porous carbon, lithium-ion battery, alkali activation

1. INTRODUCTION

With the increasing demand for energy, lithium-ion batteries with outstanding energy density, high working voltage, low self-discharge rate, green environmental protection and no memory effect have been favored by researchers, especially in the field of automotive and hybrid electric vehicles.[1, 2] The rapid development of new energy technologies has put forward higher requirements for the environmental protection and performance of electrode materials. Researchers have studied a variety of carbon materials as negative electrode for lithium-ion batteries. But with the sharp rise in the price of non-renewable fossil raw materials (such as petroleum coke and needle coke), seeking low-cost, non-polluting carbon materials has become a trend.[3-5]

Biomass wastes have a wide range of sources with a low cost. Using them as raw materials to prepare carbon materials can be cost-saving, and can alleviate environmental pollution problems caused

by a large number of incineration wastes.[6, 7] Researchers have explored a large quantity of biomass waste for energy storage, including straw, rice husks, crayfish shells, disposable wooden chopsticks, banana peel and coffee grounds, and remarkable results have been achieved.[8-13] The research results show that, compared with other waste biomass, plant fiber-derived carbon materials have a richer hierarchical porous structure, which helps to shorten the lithium-ion diffusion distance, promote electron transport, and improve cycle performance.[14]

Here, we used corn straw as a novel, inexpensive and abundant precursor to produce hierarchically porous biochar via simple KOH activation and use it as a negative electrode active material for Li-ion batteries. The study is at an advantage compared to the conventional biomass char preparation methods, mainly including the following sections. (1) Corn straw is rich in resources, so as to operate the experient in a low cost, and the environmental pollution can be reduced with the reusing of resources. (2) In terms of activation methods, the traditional template removal conditions are harsh, which not only pollutes the environment but also causes waste of chemical reagents; Chemical vapor deposition may have the risk of carbon source gas is flammable and explosive. By comparison, the KOH activation method is much more convenient and faster, thus it can multiplier the possibility of industrial production. (3) KOH has good flame retardant effect, so the oxidation of hot carbon can be prevented and the yield of biomass carbon can be improved in the carbonization activation of corn straw. Furthermore, the molten KOH also has a certain etching effect, so that the porous structure of biomass charcoal can be controlled better. In addition, as anode materials for lithium-ion batteries, the corn straw-derived carbon materials have have the advantages in stable cycling performance and large discharge capacity. Therefore, the corn straw-based porous carbon activated by KOH will surely have a wide field of application with good prospects in terms of the energy storage.

2. EXPERIMENTAL

2.1 Preparation of corn straw-based porous carbon

The corn straws are collected from Harbin City, Heilongjiang Province, northeastern China. By washing, pulverizing, and drying, they can be the carbon precursor.

Pre-carbonization stage: An appropriate amount of corn straw powder was pre-carbonized at 500 °C for 1 h (the heating rate was 5 °C/min).

Activation stage: The pre-carbonized corn straw and potassium hydroxide were uniformly mixed according to the mass ratio of 1:3 and then were placed in the tube furnace. Under the protection of the N₂ atmosphere, the sample was activated at 750 °C for 2 h (the heating rate was 5 °C/min). After cooling to room temperature, it was rinsed with 5% dilute hydrochloric acid for 1 h, then washed with deionized water until neutral, and dried under vacuum at 70 °C for 12 h. The Twice-calcined biochar after KOH activation (K-TBC) can be obtained. Twice-calcined biochar (TBC) without KOH activation was used as a control.

2.2. Sample characterization

The morphology and structure of the material were observed by scanning electron microscopy (SEM, Sigma 300). Analysis the elemental composition of materials by X-ray photoelectron spectroscopy (XPS, Thermo Fisher DXR). X-ray diffraction (XRD, D8 Advance) patterns were employed to analyze the crystal structure. The excitation wavelength of the Raman (Renishaw RM-1000) spectrum is 514.5 nm. N₂ adsorption and desorption test were carried out on 3H-2000PS1.

2.3 Electrochemical measurements

The electrochemical measurements were carried out using CR2025 coin-type cells. The working electrode was prepared by uniformly coating a slurry consisting of PVDF (polyvinylidene fluoride) and acetylene black in NMP (N-methyl pyrrolidone) solvent at a weight ratio of 8:1:1, which is consistent with the method reported in our previous work.[15]

3. RESULTS AND DISCUSSION

3.1 Microstructural characterization

Figure.1a is the SEM image of the TBC. In the absence of activator, the structure of TBC is a relatively loose lamellar structure, which may be related to the structure of the corncob itself. After adding the activator, K-TBC (Fig.1b) shows obvious etching traces, and its rich pore structure is more conducive to the adsorption of substances and the transfer of charges.

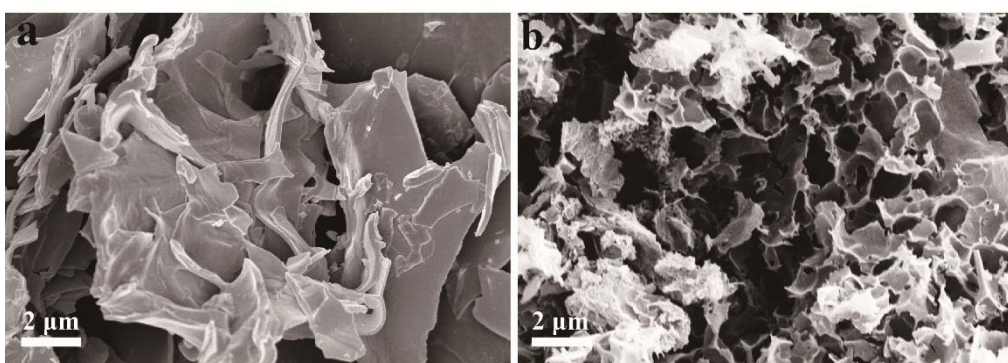


Figure 1. (a) SEM images of TBC; (b) SEM images of K-TBC.

The XRD patterns (Fig. 2a) of TBC and K-TBC show that both TBC and K-TBC have two diffraction peaks at 22° (002) and 44° (100), indicating that they have an amorphous carbon structure.[16] Compared with TBC, the (002) surface of K-TBC is wider, and the (100) surface is flatter, which means that the structure of K-TBC has been destroyed during the activation process. This would

provide K-TBC with a higher degree of graphitization and larger particle spacing, which is consistent with the SEM results.

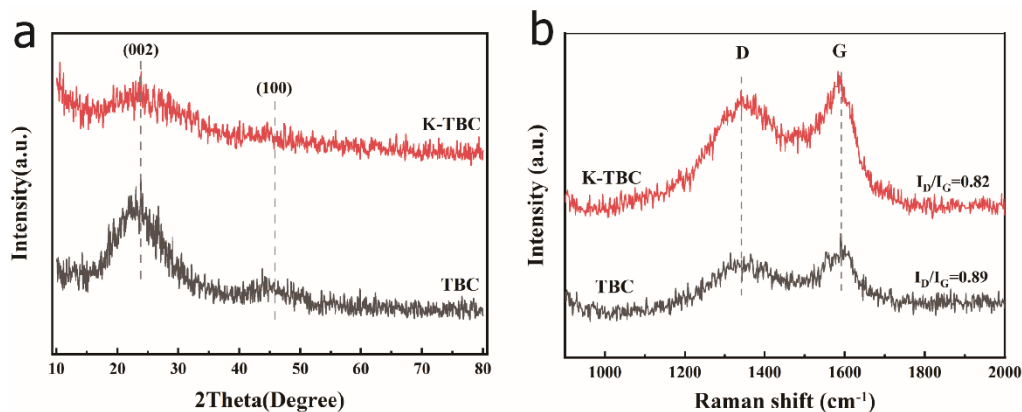


Figure 2. (a) XRD patterns of samples K-TBC and TBC; (b) Raman spectra of K-TBC and TBC.

In order to demonstrate the structural defects and the degree of rocky desertification of the activated samples, raman spectroscopy was performed on TBC and K-TBC. Figure. 2b shows that both TBC and K-TBC have distinct Raman characteristic peaks around 1350 cm^{-1} (D) and 1600 cm^{-1} (G). Among them, the D and G peaks represent the disorder degree and defect degree of the carbon material, respectively.[17] The smaller the I_D/I_G value, the higher the graphitization degree of the sample and the fewer defects.[18] With the addition of KOH, the I_D/I_G value of K-TBC decreased from 0.89 to 0.82, indicating that the addition of KOH increased the degree of graphitization of carbon materials, which is consistent with the results of XRD.

Figure 3 (a), (b), and (c) are the XPS full spectrum, C1s spectrum, and O1s spectrum of K-TBC, respectively. In the C1s spectrum of K-TBC, they correspond to C-C (284.6 eV), C-O (286.8 eV), C=O (287.3 eV), and O-C=O (289.7 eV) structures, and the O1s spectrum mainly contains C=O (287.3 eV) and O-C=O (289.7 eV) structures.[19-22] Among them, the O element mainly comes from the oxygen adsorbed by corn straw porous carbon and the oxygen in C=O, C-O, and O-C=O in functional groups. Although nitrogen was detected, its effect on the electrochemical performance was negligible due to its very low content (0.27%) and its pyrolytic loss under the action of the activator. Table 2.1 shows the C, N, and O elemental contents of TBC and K-TBC. It can be seen from the chart that the carbon-to-oxygen ratio of TBC (6.78) is greater than that of K-TBC (5.06), which indicates that KOH will reduce the carbon-to-oxygen ratio of the material at high temperatures. In contrast, in the ternary organic electrolyte system, the material with a low carbon-to-oxygen ratio with higher wettability directly increases the contract-specific surface area of the material, improving electrochemical performance.

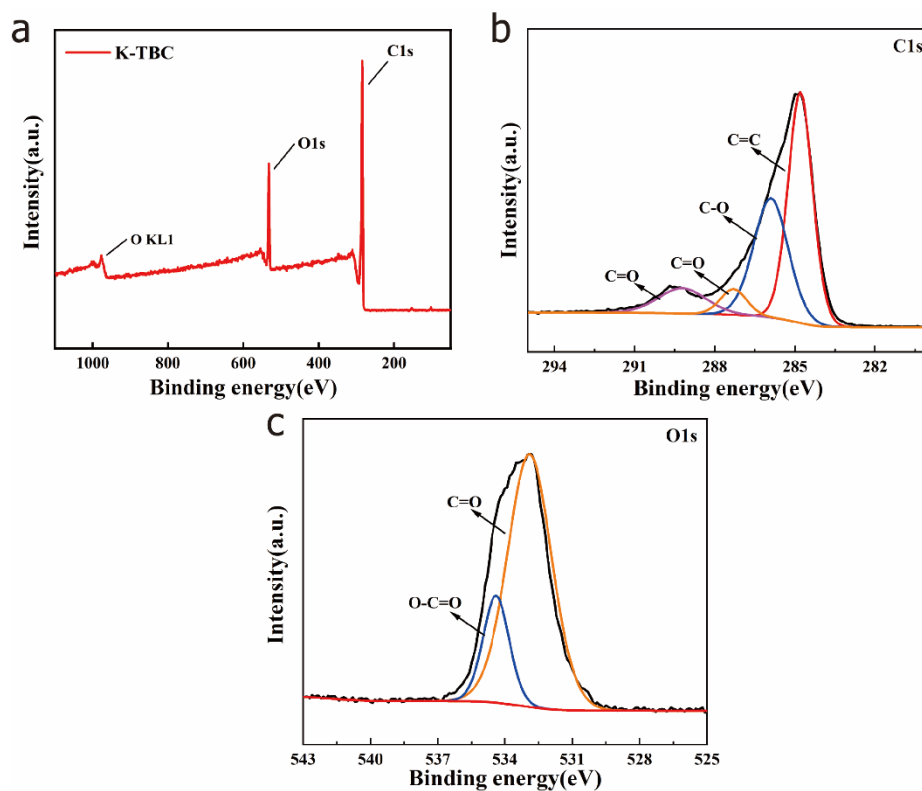


Figure 3. XPS spectras of (a) K-TBC full spectra, (b) C1s spectra, (c) O1s spectra.

Table 2.1 Element content of corn straw-based biochar.

Samples	Atomic %		
	C	O	N
K-TBC	83.27	16.46	0.27
TBC	85.46	12.59	1.95

The N adsorption and desorption isotherms of TBC and K-TBC (Fig.4a) show that the adsorption curve of TBC is type I isotherm, while the adsorption curve of K-TBC is type IV.[23] This change may be caused by the addition of the activator, the pore structure of corn straw porous carbon changed from mainly micropores to mainly mesopores. Figure. 4b shows that the pore sizes of TBCs are clustered between 1 and 2 nm, indicating that micropores dominate the material. The pore size of K-TBC is dominated by mesopores aggregated at 3-6 nm, which can provide a channel for the rapid diffusion and migration of Li^+ inside the carbon material, thereby improving the lithium-ion transport rate.

Table 2.2 Specific surface area, total pore volume and average pore size of samples.

Sample	S_{BET} (m^2g^{-1})	V_{T} (cm^3g^{-1})	D
TBC	346	0.221	2.42
K-TBC	2357	1.20	2.03

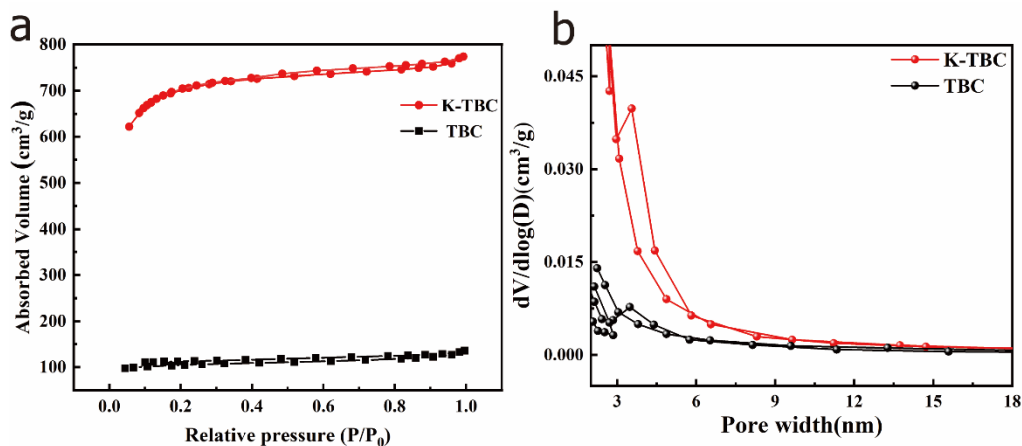


Figure 4. (a) N₂ adsorption and desorption isotherm of K-TBC and TBC; (b) pore size distribution of K-TBC and TBC.

3.2. Electrochemical properties

Coin cells were assembled with K-TBC and TBC as active materials, respectively, and the constant current charge-discharge test was carried out at 100 mA/g. The first and second galvanostatic charge-discharge curves of K-TBC and TBC (Fig. 4a) shows that the unactivated TBC has lower first charge-discharge capacities of 186 mAh/g and 450 mAh/g. When KOH activated TBC, the initial charge-discharge capacity of K-TBC was relatively good, reaching 358 mAh/g and 899 mAh/g. In addition, during the first discharge, the voltage dropped rapidly, and a discharge plateau appeared at 0.8~1.2 V, but after the second charge and discharge, the plateau disappeared. This phenomenon is due to the largely irreversible capacitance loss caused by the formation of the Solid Electrolyte Interphase (SEI) film.[24] SEI is similar to a protective wall, which can prevent excessive solvent from reacting with the electrode material, thereby protecting the electrode material, slowing down the pulverization speed, and increasing the service life of the electrode material.[25] However, due to the formation of the SEI film, the T-KBC with a larger specific surface area also needs to consume more Li ions, which also leads to more Li ions intercalated on the carbon surface, which in turn leads to a significant decrease in the specific capacity during the second discharge. Figure 5b shows the charge-discharge curves of K-TBC at the 5th, 10th, 20th, and 50th cycles. From the 5th cycle to the 50th cycle, the reversible specific capacity of K-TBC decreased from 275 mAh/g to 173 mAh/g, which may be result in the collapse of the pore structure of K-TBC carbon after repeated charge and discharge, thus affecting its charging and discharging performance.

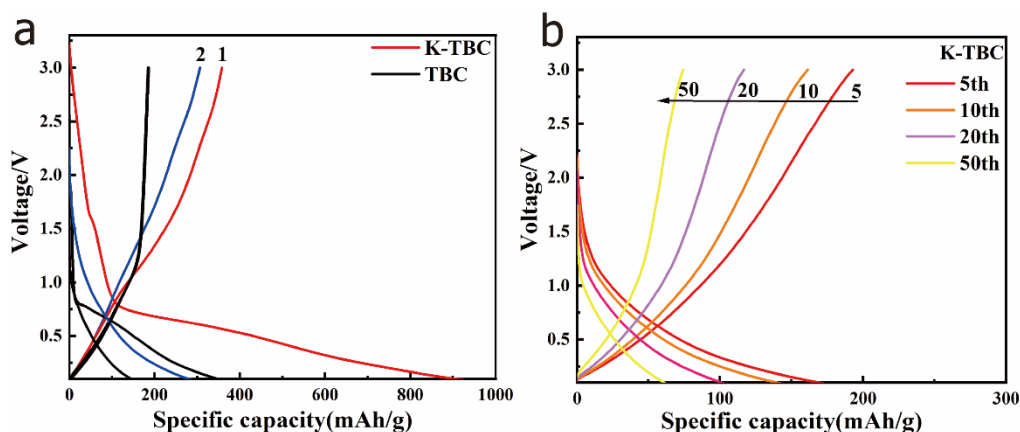


Figure 5. Charge-discharge curves of samples: (a) Charge-discharge curves of K-TBC and TBC in the first cycle and second cycle; (b) Charge-discharge curves of K-TBC.

Cyclic performance testing was performed to verify the durability of the material. Figure. 6(a) shows that the charge capacity of both TBC and K-TBC decays to around 150 mAh/g after 100 cycles. In contrast, the specific charge capacity of K-TBC (163 mAh/g) is larger than that of TBC (135 mAh/g) for the reason that K-TBC has a better pore structure and a higher degree of graphitization. The coulombic efficiency plots of K-TBC and TBC (Fig. 6b) show that the initial coulombic efficiencies of both K-TBC and TBC are relatively low, only 33.2% and 41.1%. The cycling performance of K-TBC and TBC gradually stabilized after the formation of SEI film. After 100 cycles of charge and discharge, the specific capacity of K-TBC is significantly larger than that of TBC. And the good electrochemical performance of K-TBC is mainly because of the characteristics of high degree of disorder, abundant micro-mesopores, and large specific surface area, which also shows that the study of structure and pore size distribution is of great significance in improving the electrochemical performance of anode materials. To further evaluate the lithium storage performance of K-TBC, we compared the biomass-derived electrode materials in other reports (Table 2.3). Compared with other biomass-derived electrode materials, the good reversible capacity of K-TBC enables it to be a potential electrode candidate.

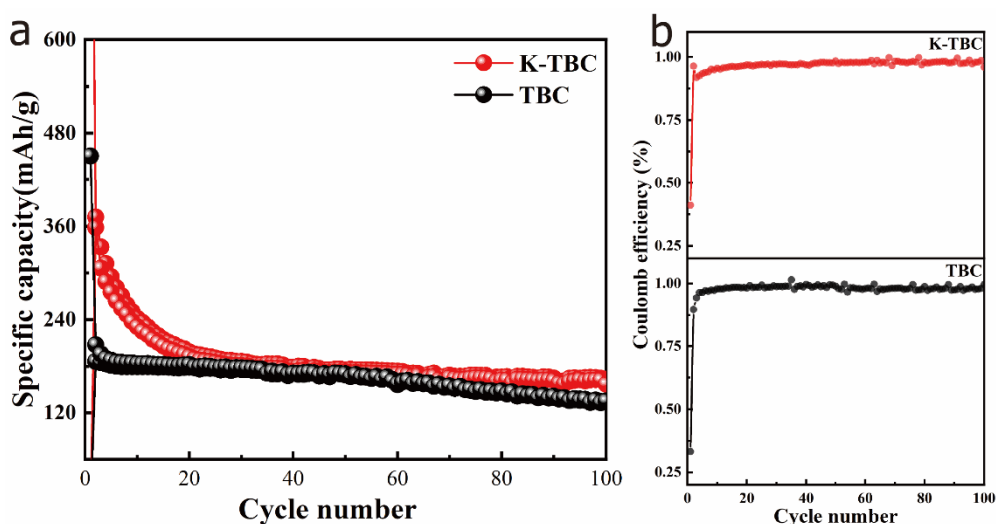
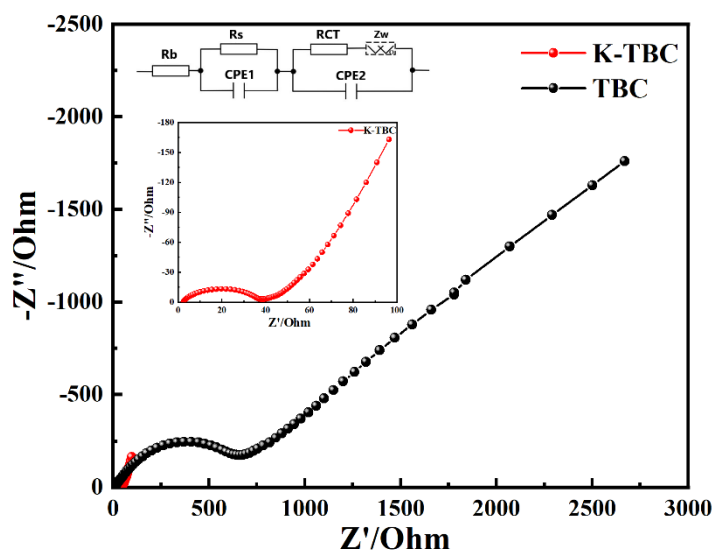


Figure 6. (a) Cycle performance of K-TBC and TBC; (b) Coulombic efficiency of K-TBC and TBC.

Table 2.3 Comparison of electrochemical performance of different biomass-derived anode materials.

Carbon precursor	Preparation method	Reversible capacity	Cycles	Reference
Corn straw	Solid-phase pyrolysis	167 mA h g ⁻¹ at 0.1 A g ⁻¹	100	This work
Seeds of Tamarindus	Solid-phase pyrolysis	163mAh g ⁻¹ at 0.2 A g ⁻¹	50	[26]
Coconut shell	Solvothermal method	120mAh g ⁻¹ at 1 A g ⁻¹	1000	[27]
camellia shells	Solvothermal method	237.6mAh g ⁻¹ at 0.1 A g ⁻¹	100	[28]
Highland barley straw	Solid-state pyrolysis	153.6mAh g ⁻¹ at 0.1 C	100	[29]
Ferrous gluconate	Solvothermal method	135.5mA g ⁻¹ at 1.0 C	100	[30]
Soybean curd	Solid-phase pyrolysis	90mA g ⁻¹ at 0.2 C	5	[31]

The Electrochemical Impedance Spectroscopy (EIS) test was performed on K-TBC and TBC at 0.1 kHz~100 kHz and 5 mV. The fitting curve simulated by Zsimpwin 3.10 is shown in Figure 7. The Nyquist curve of K-TBC to TBC consists of two semicircles and a slope close to 45°, the first semicircle corresponds to the SEI of lithium-ion batteries. As the battery ages, an electrolyte protective film will be formed on the negative electrode in lithium-ion batteries.

**Figure 7.** Nyquist plots of K-TBC and TBC. (The figure in the upper left corner is the analog equivalent circuit diagram of K-TBC.)

The formation of this protective film prevents the electrolyte ions from reaching the surface of the active material to react with lithium ions and electrons, thereby limiting the SEI film growth. Figure 7 shows that TBC has a larger resistance value, which is inseparable from the large specific surface area

and abundant pore structure of K-TBC, which is also consistent with its good electrochemical performance. In addition, to better understand the resistance value of each part, an analog equivalent circuit was established for K-TBC and TBC. From the resistance value of each part (Table 2.3), it can be found that K-TBC has excellent low impedance performance, a smaller resistance value can avoid overheating of the battery during charging and discharging, which is not only safe but also can prolong its cycle life.

Table 2.4 Fitting circuit resistance of K-TBC and TBC.

Samples	Rb(Ω)	Rs(Ω)	Rs(Ω)
K-TBC	2.26	34.85	33.02
TBC	8.2	830	520.9

4. CONCLUSIONS

We simply pulverized and activated corn stalks to prepare a porous carbon negative electrode material (K-TBC) and explored the relationship between its structure, morphology, and electrochemical lithium storage performance. The experimental results show that the porous carbon derived from corn stalk has structural characteristics such as loose structure, abundant micro-mesoporous pores, and large specific surface area, which can be positive for the high-speed transport and diffusion of ions and the increase of Li⁺ attachment sites. The K-TBC prepared by activation during secondary calcination has good electrochemical performance, and its equivalent resistance is only 2.6 Ω . At a current density of 100 mA/h, its reversible specific capacity is 358 mAh/g, much higher than that of the TBC negative electrode material prepared without activator. In addition, K-TBC also has good cycle performance. After 100 cycles of charge and discharge at 100 mA/h, the charge capacity is still 163 mAh/g, but its initial coulombic efficiency is only 41.1 %. This phenomenon is due to the destruction of the pore structure of the straw after repeated charge and discharge, as well as the low degree of graphitization. Therefore, improving the strength and graphitization degree of carbon materials also serves as the key to improving the electrochemical lithium storage performance.

ACKNOWLEDGEMENT

The work is supported by Heilongjiang Province Natural Science Foundation (no. LH2021B026) and National Natural Science Foundation of China (no. 51604102).

References

1. Y. Horowitz, C. Schmidt, D.-h. Yoon, L.M. Riegger, L. Katzenmeier, G.M. Bosch, M. Noked, Y. Ein-Eli, J. Janek, W.G. Zeier, *Energy Technology*, 8 (2020) 2000580.
2. J. Wen, D. Zhao, C. Zhang, *Renewable Energy*, 162 (2020) 1629-1648.
3. L.S. Roselin, R.-S. Juang, C.-T. Hsieh, S. Sagadevan, A. Umar, R. Selvin, H.H. Hegazy, *Materials*, 12 (2019) 1229.

4. Y. Chen, X. Guo, A. Liu, H. Zhu, T. Ma, *Sustainable Energy & Fuels*, 5 (2021) 3017-3038.
5. X. Tang, D. Liu, Y.-J. Wang, L. Cui, A. Ignaszak, Y. Yu, J. Zhang, *Progress in Materials Science*, 118 (2021) 100770.
6. A. Benítez, J. Amaro-Gahete, Y.-C. Chien, Á. Caballero, J. Morales, D. Brandell, *Renewable and Sustainable Energy Reviews*, 154 (2022) 111783.
7. S.K. Tiwari, M. Bystrzejewski, A. De Adhikari, A. Huczko, N. Wang, *Progress in Energy and Combustion Science*, 92 (2022) 101023.
8. K. Yu, B. Wang, P. Bai, C. Liang, W. Jin, *Journal of Electronic Materials*, 50 (2021) 6438-6447.
9. S. Kumagai, Y. Abe, M. Tomioka, M. Kabir, *Scientific Reports*, 11 (2021) 1-13.
10. H. McKinley, Tulane University School of Science and Engineering 2021.
11. J. Yu, T. Tang, F. Cheng, D. Huang, J.L. Martin, C.E. Brewer, R.L. Grimm, M. Zhou, H. Luo, *Materials Today Energy*, 19 (2021) 100580.
12. S.J. Hong, S.S. Kim, S. Nam, *Corrosion Science and Technology*, 20 (2021) 15-21.
13. F. Luna-Lama, J. Morales, A. Caballero, *Materials*, 14 (2021) 5995.
14. G. Jiang, R.A. Senthil, Y. Sun, T.R. Kumar, J. Pan, *Journal of Power Sources*, 520 (2022) 230886.
15. L. Liu, M. An, P. Yang, J. Zhang, *Scientific reports*, 5 (2015) 1-10.
16. B. Manoj, A. Kunjomana, *Int. J. Electrochem. Sci.*, 7 (2012) 3127-3134.
17. M. Pimenta, G. Dresselhaus, M.S. Dresselhaus, L. Cancado, A. Jorio, R. Saito, *Physical chemistry chemical physics*, 9 (2007) 1276-1290.
18. R. Escribano, J. Sloan, N. Siddique, N. Sze, T. Dudev, *Vibrational Spectroscopy*, 26 (2001) 179-186.
19. N.J. Song, C. Ma, P. Li, W. Li, F. Guo, Y. Du, Y. Chen, *International Journal of Energy Research*, (2022).
20. R. Atchudan, K. Samikannu, S. Perumal, T.N.J.I. Edison, R. Vinodh, Y.R. Lee, *Materials Letters*, 309 (2022) 131445.
21. C.C. Roldán, A. Ayala-Cortés, R. González-Huerta, H. Villafán-Vidales, C. Arancibia-Bulnes, A. Cuentas-Gallegos, M. Farías, D. Martínez-Casillas, *International Journal of Hydrogen Energy*, 46 (2021) 26101-26109.
22. S. Breitenbach, N. Gavrilov, I. Pašti, C. Unterweger, J. Duchoslav, D. Stifter, A.W. Hassel, C. Fürst, *C*, 7 (2021) 55.
23. N. Rajamohan, F.S.Z.S. Al Shibli, *Chemosphere*, 292 (2022) 133479.
24. Y. Liu, M. Shi, C. Yan, Q. Zhuo, H. Wu, L. Wang, H. Liu, Z. Guo, *Journal of Materials Science: Materials in Electronics*, 30 (2019) 6583-6592.
25. Y. Li, C. Li, H. Qi, K. Yu, X. Li, *RSC advances*, 8 (2018) 12666-12671.
26. M.R. Panda, A.R. Kathribail, B. Modak, S. Sau, D.P. Dutta, S. Mitra, *Electrochimica Acta*, 392 (2021) 139026.
27. A.J. Jiao, J.F. Gao, Z.H. He, F.F. Li, L.B. Kong, *ChemistrySelect*, 6 (2021) 8349-8360.
28. S. Chen, K. Tang, F. Song, Z. Liu, N. Zhang, S. Lan, X. Xie, Z. Wu, *Nanotechnology*, 33 (2021) 055401.
29. W. Sun, R. Hao, *INTERNATIONAL JOURNAL OF ELECTROCHEMICAL SCIENCE*, 16 (2021).
30. J. Lan, H. Hou, K. Meng, M. Feng, J. Li, *Electrochimica Acta*, 390 (2021) 138827.
31. A. Hardiansyah, E.R. Chaldun, B.W. Nuryadin, A.K. Fikriyyah, A. Subhan, M. Ghozali, B.S. Purwasasmita, *Journal of Electronic Materials*, 47 (2018) 4028-4037.